

# The multiferroic phases of $\text{Eu}_{1-x}\text{Y}_x\text{MnO}_3$

J. Hemberger<sup>1</sup>, F. Schrettle<sup>1</sup>, A. Pimenov<sup>1</sup>, P. Lunkenheimer<sup>1</sup>,  
V.Yu. Ivanov<sup>2</sup>, A.A. Mukhin<sup>2</sup>, A.M. Balbashov<sup>3</sup>, and A. Loidl<sup>1</sup>

<sup>1</sup>*Experimentalphysik V, Center for Electronic Correlations and Magnetism,  
University of Augsburg, D-86135 Augsburg, Germany*

<sup>2</sup>*General Physics Institute of the Russian Academy of Sciences, 38 Vavilov Street, 119991 Moscow, Russia*

<sup>3</sup>*Moscow Power Engineering Institute, 14 Krasnokasarmennaja Street, 111250 Moscow, Russia*

We report on structural, magnetic, dielectric, and thermodynamic properties of  $\text{Eu}_{1-x}\text{Y}_x\text{MnO}_3$  for Y doping levels  $0 \leq x < 1$ . This system resembles the multiferroic perovskite manganites  $\text{RMnO}_3$  (with  $R = \text{Gd}, \text{Dy}, \text{Tb}$ ) but without the interference of magnetic contributions of the  $4f$ -ions. In addition, it offers the possibility to continuously tune the influence of the  $A$ -site ionic radii. For small concentrations  $x \leq 0.1$  we find a canted antiferromagnetic and paraelectric groundstate. For higher concentrations  $x \geq 0.3$  ferroelectric polarization coexists with the features of a long wavelength incommensurate spiral magnetic phase analogous to the observations in  $\text{TbMnO}_3$ . In the intermediate concentration range around  $x \approx 0.2$  a multiferroic scenario is realized combining weak ferroelectricity and weak ferromagnetism, presumably due to a canted spiral magnetic structure.

PACS numbers: 71.45.Gm, 75.30.-m, 75.30.Kz, 77.84.Bw, 77.90.+k

## I. INTRODUCTION

In recent years multiferroics have attracted an increasing scientific and technological interest in the large community working on functional transition-metal compounds.<sup>1</sup> Within this rare class of materials magnetic order coexists with long range polar order and both order-parameters are strongly coupled. Prominent examples for such multiferroics may be found among Cr-based spinels<sup>2,7</sup>, the kagomé staircase compound  $\text{Ni}_3\text{V}_2\text{O}_8$ <sup>4</sup>, rare earth manganites like hexagonal  $\text{YMnO}_3$  and  $\text{HoMnO}_3$ <sup>5,6</sup>, orthorhombic  $\text{TbMn}_2\text{O}_5$ <sup>7</sup>, or finally perovskites like  $\text{TbMnO}_3$ .<sup>8</sup>

In this latter class of heavy rare earth compounds  $\text{RMnO}_3$  ( $R = \text{Gd}, \text{Tb}, \text{Dy}$ )<sup>9,10</sup> finite ferroelectric polarization is induced due to the partial frustration and corresponding long range modulation of the magnetic structure. The importance of the Dzyaloshinskii-Moriya interaction for the occurrence of ferroelectricity in non-collinear magnets has been pointed out recently.<sup>11,12,13</sup> Starting from the lanthanide manganite with the perovskite tolerance factor close to unity, the substitution of La at the  $A$ -sites by rare-earth elements with smaller ionic radii (from Pr to Ho) leads to a successive increase of the orthorhombic distortion, accompanied by a decrease of the Mn-O-Mn bond angles and an increase of the buckling and tilting angles of the  $\text{MnO}_6$ -octahedra, respectively.<sup>9</sup> Using high-resolution x-ray diffraction and the refinement of the oxygen positions, this angle has recently been determined for the complete series of pure rare-earth manganites.<sup>8</sup> Equivalent results can be obtained when continuously replacing  $\text{La}^{3+}$  by smaller ions like in  $\text{La}_{1-y}\text{Gd}_y\text{MnO}_3$ .<sup>14</sup> The enhanced tilting of the  $\text{MnO}_6$ -octahedra leads to an increasing importance of antiferromagnetic (AFM) next-nearest neighbor interactions competing with the nearest neighbor superexchange within the ferromagnetic (FM)  $ab$ -planes of the  $A$ -type AFM structure. This weakening of the effective magnetic

interaction promotes a tendency towards frustration and complex spin-states.<sup>15</sup> Hence, the transition temperature into the  $A$ -type AFM phase is not only reduced, but for the heavy rare earth compounds with smaller ionic radii an incommensurate magnetic structure is established for temperatures below  $T_N \approx 50$  K.<sup>14,15</sup> Within these incommensurate magnetic phases, magnetoelectric coupling via long-range modulation of the magnetic structure leads to the loss of inversion symmetry and the onset of ferroelectric polarization.<sup>16</sup> The onset of ferroelectricity is connected with the change of the magnetic structure from a sinusoidal to a helicoidal modulation.<sup>16,17</sup> Very recently excitations of the multiferroic state have been observed experimentally.<sup>18</sup> These new collective modes, which are responsible for ferroelectricity, but are of magnetic origin, have also been described theoretically.<sup>19</sup> The existence of a ferroelectric lattice distortion is especially remarkable due to the fact that these compounds possess a quite robust Jahn-Teller (JT) type orbital order, which sets in at temperatures well above 1000 K. From a principal point of view Jahn-Teller active orbital degrees of freedom are the "natural enemy" of off-center ferroelectric distortions.<sup>20</sup> Undistorted orbital electron-density distributions are point-symmetric carrying no electric dipole moment. Hence, if the lattice is able to relax into a lower symmetry via a Jahn-Teller distortion this transition is expected not to be dipolar. In this sense the ferroelectricity in the heavy rare earth manganites exists not due to, but despite the superimposed orbital order and comparing the relevant energy scales it has to be regarded as a second order effect. Therefore the ferroelectric distortion is rather weak and so far could not be proven directly using high-resolution neutron or x-ray diffraction techniques. However, the onset of ferroelectricity was documented via pyroelectric measurements and is connected to a distinct anomaly in the real part of the dielectric permittivity<sup>10</sup> and clear features in the anisotropic thermal expansion.<sup>21</sup> This underlines that the ferroelectric

distortions are driven by frustrated magnetic interactions via local exchange-striction.<sup>8</sup>

However, within the scenario of partially frustrated Mn-spins the role of the magnetic  $A$ -sites is not completely clear so far. Generally, the moments of the rare-earth ions are polarized due to the coupling with the Mn subsystem resulting in a noticeable anisotropic contribution to the low-temperature magnetic and thermodynamic properties of the manganites as e.g. recently studied in detail for the systems  $\text{PrMnO}_3$  and  $\text{NdMnO}_3$ .<sup>22</sup> As analyzed for the case of  $\text{TbMnO}_3$  by Quezel *et al.*<sup>17,23</sup> the overall magnetic structure in the rare-earth manganites can be rather complex. They found a sine-wave ordering of the  $\text{Mn}^{3+}$  moments with the ordering wave vector along the  $b$ -axis below 40 K and a short-range incommensurate ordering of the  $\text{Tb}^{3+}$  moments with a different wave vector below 7 K. At the ordering temperature of the rare-earth moments significant anomalies in the dielectric constant can be found denoting the possible influence of the magnetic  $A$ -sites.<sup>10</sup>

In this paper we report structural, magnetic susceptibility, magnetization, and specific heat measurements for single and poly-crystalline  $\text{Eu}_{1-x}\text{Y}_x\text{MnO}_3$ . Our focus is directed towards the isovalent doping of the trivalent  $A$ -site in  $\text{RMnO}_3$ , with  $R$  denoting elements  $\text{Eu}^{3+}$  ( $4f^8$ ) or  $\text{Y}^{3+}$  ( $[\text{Kr}]$ ).<sup>24</sup> This allows for a systematic variation of the ionic radii and possibly of the Mn-O-Mn angle, which we relate to the development of the complex magnetic groundstates and ferroelectric phases analogous to the pure rare-earth compounds  $\text{RMnO}_3$  with  $R = \text{Gd}, \text{Dy}, \text{Tb}$ . The system  $(\text{Eu}:\text{Y})\text{MnO}_3$  offers the possibility to *continuously* control the  $A$ -site volume of the orbitally ordered perovskite structure and thus to tune the corresponding multiferroic phases without the additional influence of a magnetic rare earth moment. A further aspect of the system  $\text{Eu}_{1-x}\text{Y}_x\text{MnO}_3$  is the robustness of long-range polar order against the influence of purely structural  $A$ -site disorder.

## II. EXPERIMENTAL DETAILS

$\text{Eu}_{1-x}\text{Y}_x\text{MnO}_3$  single crystals were grown in Ar flow by a floating-zone method with radiation heating for Y-concentrations  $x = 0, 0.1, 0.2, 0.3$ , and 0.5. Additional concentrations have been prepared as poly-crystals for higher concentrations up to  $x = 0.95$  using conventional solid state reaction methods. Powder-diffraction experiments were performed on powder of crushed single and poly-crystals at room temperature with a STOE diffractometer utilizing  $\text{Cu-K}\alpha$  radiation with a wave length  $\lambda = 0.1541$  nm. The magnetic susceptibility and the magnetization were recorded using a commercial SQUID magnetometer for temperatures  $T < 400$  K and external magnetic fields up to 50 kOe. The dielectric constant has been measured employing a frequency response analyzer (NOVOCONTROL  $\alpha$ -ANALYZER and HP4284A ) and the spontaneous electric polarization was recorded as inte-

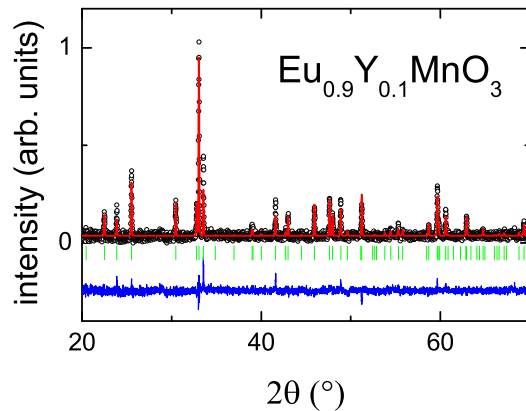


FIG. 1: (Color online) Representative powder XRD-Pattern for the  $\text{Eu}_{0.9}\text{Y}_{0.1}\text{MnO}_3$ . The lines show the results of a Rietveld refinement (upper line through the data points) and the corresponding deviation from the experimental data (below the data). The bars in between denote reflections of the Pbnm structure.

grated pyro-current. The specific heat was measured in a PPMS-system (QUANTUM-DESIGN).

## III. RESULTS AND DISCUSSION

### A. Structure

A typical result for the structural characterization of the samples by x-ray diffraction is shown in Fig. 1. The diffraction patterns were refined using Rietveld analysis. All samples investigated revealed the O' orthorhombic structure (Pbnm). No impurity phases were detected above background level for Y-concentrations  $x < 0.75$ . For higher concentrations (as denoted in Fig. 2), small traces of the hexagonal (P63cm) phase of  $\text{YMnO}_3$  show up which could be estimated to be below 2 % and will not considerably influence the regarded macroscopic properties. The lattice constants and the volume of the unit cell as derived from the profile analysis are shown in Fig. 2. In addition, the data for the system  $\text{La}_{1-y}\text{Gd}_y\text{MnO}_3$ , which was taken from Ref. [14], is displayed on a separate scale. Both scales, for Gd-doping  $y$  and Y-doping  $x$  are shifted to achieve an overlap of the structural data. For all concentrations we find  $b > a > c/\sqrt{2}$  indicative for a static JT distortion superimposed on the high temperature O-type (i.e. not JT distorted) orthorhombic structure, which results from the buckling and tilting of the  $\text{MnO}_6$  octahedra due to geometrical constraints. However, for  $\text{Eu}_{1-x}\text{Y}_x\text{MnO}_3$ , despite the continuous shrinking of the lattice volume  $V$ , the orthorhombic distortion parameterized by  $\varepsilon = (b - a)/(a + b)$  tends to saturate for higher Y-concentrations. The inequality of the lattice constants  $a$  and  $b$  reflects the tilting of the octahedra around the  $b$ -axis and implies significant deviations from  $180^\circ$  of the Mn-O-Mn bond angle  $\phi$  within the  $ab$ -

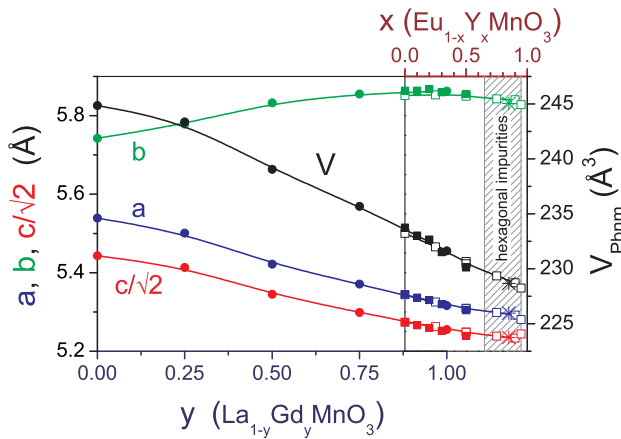


FIG. 2: (Color online) Lattice constants  $a$ ,  $b$ , and  $c/\sqrt{2}$  (left scale) and volume of the unit cell (right scale) in  $\text{Eu}_{1-x}\text{Y}_x\text{MnO}_3$  and  $\text{La}_{1-y}\text{Gd}_y\text{MnO}_3$  vs. concentration of Y ( $x$ , upper scale, squares) and Gd ( $y$ , lower scale, circles). Both scales are shifted to adapt the overlap of the data. The solid symbols represent data evaluated from regrinded single crystals, the open symbols represent data evaluated from polycrystalline material. The asterisks denote the lattice parameters of pure  $\text{TbMnO}_3$  which are placed to match the values of  $\text{Eu}_{1-x}\text{Y}_x\text{MnO}_3$  close to  $x \approx 0.85$ . Within the hatched area small traces of hexagonal impurity phases (< 2%) have been detected.

plane. Another quantity reflecting the development of  $\phi$  is the tilting distortion along  $b$  of the  $A$ -site as obtained from the Rietveld refinement of the atomic positions. This parameter (not shown) is almost constant for the system  $\text{Eu}_{1-x}\text{Y}_x\text{MnO}_3$  in contrast to the less distorted system  $\text{La}_{1-y}\text{Gd}_y\text{MnO}_3$ .<sup>14</sup> This implies, that the alteration of the spin system due to the influence of the Mn-O-Mn bond angle may not be the only valid mechanism for  $\text{Eu}_{1-x}\text{Y}_x\text{MnO}_3$ . In addition, the variation of the magnetic exchange via the reduction of the volume and the corresponding changes in the orbital overlap may also have to be considered. Also the  $A$ -site disorder and the corresponding variance in the  $A$ -site ionic radii could play an important role. The asterisks in Fig. 2 display the structural parameters of pure  $\text{TbMnO}_3$ .<sup>23</sup> The data agree with the findings for the Y-concentration  $x \approx 0.85$ . If only taking into account the averaged ionic radii, the values of the Tb-system should be located at  $x \approx 0.4$ .<sup>25</sup> For the system  $\text{GdMnO}_3$  an equivalent concentration of  $x \approx 0.3$  is found while the value is expected to be  $x \approx 0.15$ . This shows that for  $\text{Eu}_{1-x}\text{Y}_x\text{MnO}_3$  the lattice is less contracted than it would be expected compared to the pure rare earth manganites.

## B. Magnetism

Fig. 3 shows the magnetic DC susceptibilities  $\chi = M/H$  for concentrations  $x \leq 0.5$ . At elevated temperatures all susceptibilities follow a Curie-Weiss (CW) law

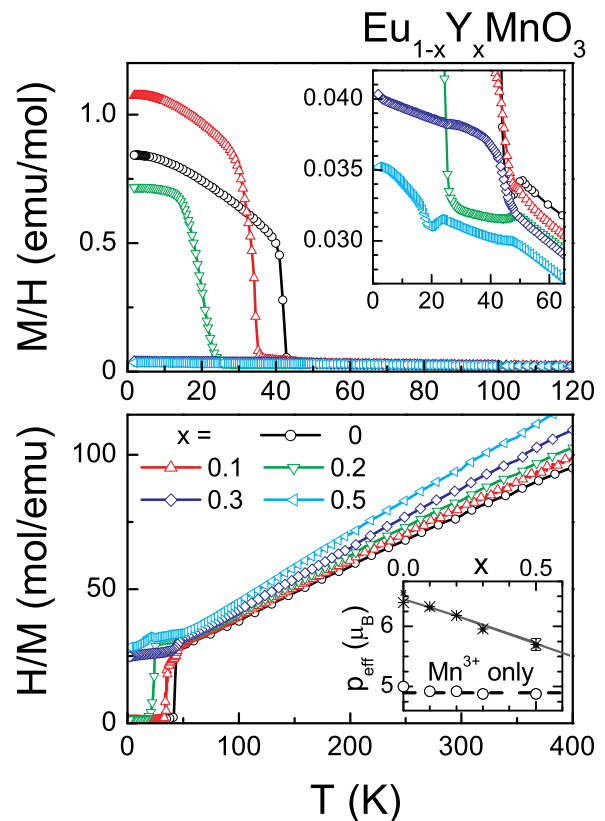


FIG. 3: (Color online) Temperature dependence of the magnetic DC-susceptibility  $\chi = M/H$  (upper frame, for  $T < 100$  K) and the inverse DC-susceptibility  $1/\chi = H/M$  (lower frame, for  $T < 400$  K) for various concentrations of  $\text{Eu}_{1-x}\text{Y}_x\text{MnO}_3$  as measured along  $c$  in an external magnetic field of 1 kOe. The upper inset provides an expanded view of  $M/H$  close to the magnetic phase transitions. The lower inset shows the effective paramagnetic moment  $p_{\text{eff}}$  as obtained from a simple Curie-Weiss type evaluation (\*) of the linear regime of  $1/\chi$  above  $T = 100$  K and from an analysis separating the contributions of Eu and Mn as described in the text (o).

as revealed by the inverse representation in the lower frame of Fig. 3. The corresponding effective paramagnetic moments  $p_{\text{eff}}$  are plotted in the lower inset of Fig. 3 (\*).  $p_{\text{eff}}$  is decreasing due to the decreasing rare-earth contribution.  $\text{Y}^{3+}$  is nonmagnetic and for  $\text{Eu}^{3+}$  the  $4f^6$ -configuration leads to  $J = 0$ . However, for Eu low-lying multiplets give rise to a Van-Vleck type of contribution, which in this temperature regime is nearly Curie-like and thus enhances the effective paramagnetic moment. For a more detailed analysis the paramagnetic high temperature behavior was fitted by a sum of the contribution of  $\text{Eu}^{3+}$  ( $\propto (1-x)$ ) and the CW type contribution of  $\text{Mn}^{3+}$ . For the Eu-contribution we used the well known free ion susceptibility of  $\text{Eu}^{3+}$  determined by its excited multiplets with  $E_1 \approx 500$  K and  $E_2 \approx 3E_1$  for  $J = 1$  and  $J = 2$ , respectively.<sup>26,27</sup> At high temperatures it is linear in  $1/T$  while at low  $T$  it is determined by a temperature

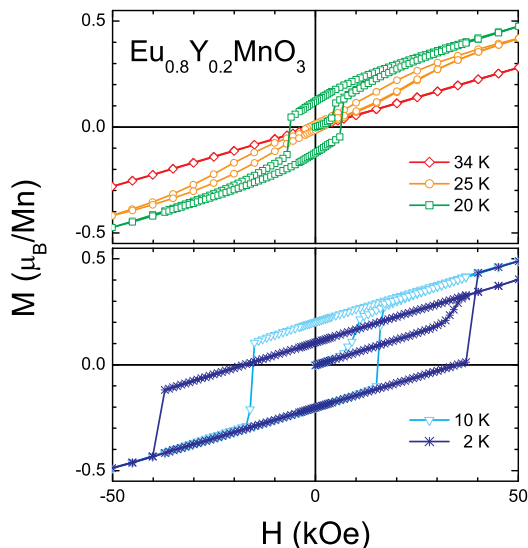


FIG. 4: (Color online) Magnetization along  $c$  of  $\text{Eu}_{0.8}\text{Y}_{0.2}\text{MnO}_3$  as function of the external magnetic field for a series of temperatures between 2 K and 34 K.

independent Van-Vleck contribution. All our data can be nicely described using  $p_{\text{eff,Mn}}$  as plotted in the lower inset of Fig. 3 (○). The manganese contribution turns out to be independent of  $x$  and agrees well with the expected theoretical value  $2\mu_B\sqrt{[S(S+1)]} = 4.9\mu_B$ . For concentrations  $x \leq 0.5$  the CW-temperatures of the Mn-subsystem are  $\Theta \approx -58 \pm 4$  K and are almost independent of  $x$ . This result is in agreement with corresponding findings in  $\text{La}_{1-y}\text{Gd}_y\text{MnO}_3$  for high Gd concentrations.<sup>14</sup>

Below 50 K all compositions undergo a magnetic transition into an incommensurate antiferromagnetic (IC) phase as concluded in analogy to the pure rare earth compounds.<sup>9</sup> This transition was clearly detected by heat-capacity experiments, which will be discussed later. It can only be seen as a small change of slope in the temperature dependence of the magnetic susceptibility as it is not connected with the onset of a ferromagnetic component (see upper inset of Fig. 3). A much stronger anomaly appears at the transition from the incommensurate magnetic state into the canted A-type antiferromagnetic (CAF<sub>M</sub>), which takes place for concentrations  $x \leq 0.3$ . As revealed by the upper frame of Fig. 3, the onset of CAF<sub>M</sub> order at  $T_{\text{CAF<sub>M shows up as a strong upturn of magnetization indicating a significant ferromagnetic contribution. This FM component arises due to spin canting, which can be explained by the Dzyaloshinsky-Moriya interaction and is an intrinsic feature of the CAF<sub>M</sub> state in  $R\text{MnO}_3$  systems.<sup>28,29</sup> As stated above,  $T_{\text{CAF<sub>M continuously decreases from 140 K in  $\text{LaMnO}_3$  down to about 20 K in  $\text{GdMnO}_3$ . For the system  $\text{Eu}_{1-x}\text{Y}_x\text{MnO}_3$  this transition is shifted to  $T \approx 0$  for Y-concentrations of about  $0.2 \leq x \leq 0.3$ . For  $\text{TbMnO}_3$  and for concentrations  $x \geq 0.3$  in  $\text{Eu}_{1-x}\text{Y}_x\text{MnO}_3$  no A-type AFM can be found but the character of the mag-</sub>$</sub>$

netic phase changes from a sinusoidal to a helicoidal (spiral) magnetic structure at temperatures between 20 and 30 K.<sup>17</sup> This latter transition is connected with the onset of ferroelectric order as will be discussed later. However, it still seems a controversial debate if this spiral AFM structure remains incommensurate<sup>17</sup> or locks-in at a commensurate wave vector.<sup>30</sup> It should be noted that at least for the composition  $x = 0.5$  additional small anomalies can be found at the FE transitions at 24 K and 18 K, indicative for a partial rearrangement of the magnetic structure.

Fig. 4 shows the magnetization  $M(H)$  for  $\text{Eu}_{0.8}\text{Y}_{0.2}\text{MnO}_3$  in magnetic fields up to 5 T as measured after zero-field cooling. At  $T = 34$  K (upper frame of Fig. 4) an apparently paramagnetic magnetization behavior is detected. As can be deduced from the specific heat data (presented below) the magnetic state of the sample at this temperature is in fact the IC phase. At 25 K the CAF<sub>M</sub> state can be induced by the magnetic field as reflected by the twofold hysteresis loop with the typical signature of a smeared out metamagnetic phase transition at  $H \approx 30$  kOe. On further decreasing temperature this metamagnetic transition becomes fully irreversible and the two loops are merged into one as it is characteristic for a weak ferromagnet. After the initial increase of the field the CAF<sub>M</sub> state persists and only the ferromagnetic component is switched at a sharply defined coercive field, which increases up to  $H_c \approx 40$  kOe for the lowest temperatures. At 2 K (lower frame of Fig. 4) even an intermediate state with a smaller ferromagnetic component is stabilized after the initial increase of the magnetic field leading to an asymmetric shape of the hysteresis loop.

### C. Dielectric properties

Fig. 5 displays the real part of the dielectric constant as measured in the radio-frequency range for various concentrations of  $\text{Eu}_{1-x}\text{Y}_x\text{MnO}_3$ . All  $\epsilon'(T)$  curves show a steplike increase with increasing temperature along the  $c$ -direction. Its point of inflection is located around 50 K but as shown exemplarily for the concentration  $x = 0.5$  (lower right frame of Fig. 5) its position is strongly frequency dependent. Similar phenomena have already been found e.g. for  $\text{TbMnO}_3$  and have been ascribed to the relaxation of localized polarons.<sup>8</sup> In the following we will concentrate on the anomalies below 45 K. For pure  $\text{EuMnO}_3$  only a tiny kink can be found near  $T \approx 43$  K. This coincides with the onset of weak ferromagnetism in the CAF<sub>M</sub> phase as revealed from the magnetic susceptibility measurements. For  $x = 0.2$  a similar anomaly at  $T_{\text{CAF<sub>M K can be observed, which can hardly be recognized, but a much more prominent peak occurs at 30 K. For  $x = 0.3$  this anomaly is located at 26 K and for  $x = 0.5$  it forms a double-peak structure at roughly 23 K and 19 K. A similar double structured peak can also be detected along the  $a$ -direction, however with shifted</sub>$

weight from higher to the lower temperature peak. These anomalies in  $\varepsilon'(T)$  coincide with the onset of ferroelectricity as will be described later. For the concentrations  $x = 0.2, 0.3,$  and  $0.5$  the electric polarization  $P(T)$  is shown in Fig. 6. As revealed by the uppermost frame of Fig. 6, obviously the double structure in  $\varepsilon'(T)$  for  $\text{Eu}_{0.5}\text{Y}_{0.5}\text{MnO}_3$  (lower right frame of Fig. 5) corresponds to the partial spontaneous reorientation of  $P$  from the  $c$ - to the  $a$ -direction. This is in accord with recent results obtained for  $x \approx 0.4$  by Kuwahara and coworkers.<sup>25</sup> Such a spontaneous reorientation of the electric polarization is not reported for the pure systems  $\text{RMnO}_3$ .<sup>10</sup> For the compositions  $\text{Eu}_{1-x}\text{Y}_x\text{MnO}_3$  with  $x = 0.3$  and  $0.2$  no temperature dependent reorientation of the polarization could be observed as it is shown in the lower frames of Fig. 6. It is remarkable that despite the magnetoelectric origin of the FE order no clear anomaly in  $P(T)$  can be observed for  $x = 0.2$  around 23 K where a spontaneous FM component sets in. However, as can be seen from Fig. 4 the values for the spontaneous magnetization stay below  $0.2\mu_B$  per  $\text{Mn}^{3+}$  ion. This is only 1/20th of the maximal ordered moment of  $4\mu_B$ . Thus the effective FM moment can be explained by a canting of the presumably spiral magnetic structure of less than  $3^\circ$ , which represents an only small modification of the magnetic structure.

Ferroelectricity (FE) does not occur for concentrations

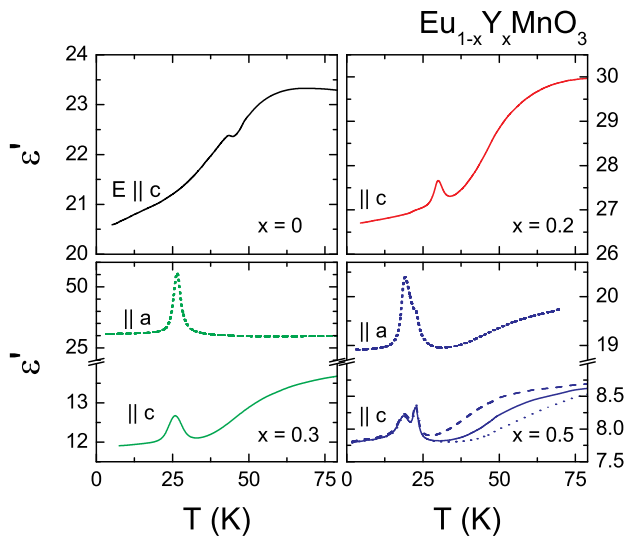


FIG. 5: (Color online) Temperature dependence of the real part of the permittivity  $\varepsilon'$  for the Y-concentrations  $x = 0, 0.2, 0.3,$  and  $0.5$  as measured at  $\nu = 100$  kHz. The lower right frame ( $x = 0.5$ ) shows additional data for the frequencies 27 kHz (dashed) and 250 kHz (dotted). Additional data for  $E||a$  is given for the concentrations  $x = 0.3$  and  $0.5$  (lower frames, short dashes). In general, the measured data of  $\varepsilon'$  may comprise a constant additional contribution due to stray capacitance of the measurement setup together with an relative uncertainty of up to 25 % due to the determination of the sample geometry. Hence, the absolute values of  $\varepsilon'(T)$  are not discussed. However, the relative accuracy of the measurement is much higher and lies within the thickness of the lines.

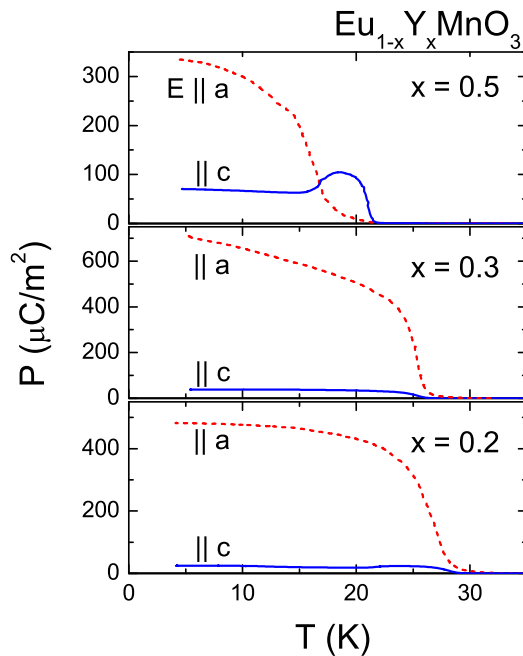


FIG. 6: (Color online) Electric polarization as measured on heating after cooling down in a poling field of about 100 V/mm for the Y-concentrations  $x = 0.2, 0.3,$  and  $0.5$ .

below  $x < 0.2$ . Nevertheless, it is remarkable that a canted, i.e. weakly ferromagnetic state and FE are not mutually exclusive. For  $x = 0.2$  the system first becomes ferroelectric at  $T_{\text{FE}} \approx 30$  K and then the ferromagnetism evolves roughly 8 K below. In a strict sense, this is the only multiferroic system among the rare earth perovskite manganites where the ground state seems to combine the properties of ferromagnetism and ferroelectricity. The most prominent examples like  $\text{TbMnO}_3$  never show a finite spontaneous FM and FE order-parameter at the same time.

#### D. Specific heat

Fig. 7 presents the results of heat-capacity measurements in  $\text{Eu}_{1-x}\text{Y}_x\text{MnO}_3$  as function of temperature. The heat capacity, plotted as  $C/T$ , is shown for temperatures  $T < 65$  K and concentrations  $0 \leq x \leq 0.5$ . A well defined lambda-like anomaly shows up between 45 K and 50 K for all concentrations under investigation. In agreement with magnetization data and deduced from observations in other rare-earth manganites this anomaly has to be interpreted as onset of the IC spin structure, which gives no macroscopic FM moment.<sup>8</sup> The transition temperature is slightly decreasing with increasing Y-concentration. Below 45 K for each concentration a further anomaly appears at lower temperatures which for pure  $\text{EuMnO}_3$  is characterized by a sharp peak in  $C/T$  at 44 K corresponding to the transition into the A-type AFM-phase (see

Fig. 3). For the Y doped samples this feature gets considerably smeared out presumably due to the influence of disorder. Again the corresponding transition temperature as denoted by the onset of the broad shoulder-like contribution is monotonously decreasing with increasing  $x$  down to about 20 K for  $x = 0.5$ . However, even though the shape of this anomaly in  $C/T$  is not altered qualitatively, the corresponding transition refers to different ground states for different compositions. As it was already revealed in Figs. 3 and 6 the onset of spontaneous magnetization corresponds to the transition into a new magnetic ground state with FM and FE components for concentrations  $x \approx 0.2$ . For higher concentrations the spiral IC structure persists down to lowest temperatures in analogy to the pure rare earth compounds, but the onset of a FE polarization corresponds to a change from a sinusoidal to a helicoidal magnetic structure.<sup>17</sup> The absence of any qualitative differences in the curvature of  $C/T$  for the different compositions reflects that the corresponding ground states together with their partially frustrated spin structures are nearly degenerate.

It is worth mentioning that the low temperature specific heat in this system differs essentially from that of  $\text{GdMnO}_3$  or  $\text{TbMnO}_3$  due to the missing contribution of the magnetic rare earths.<sup>8,14</sup> Neither a Schottky-type contribution as found due to the rare earth spins, which are polarized in the effective exchange field from the CAFM Mn-sublattice, nor an anomaly due to the subsequent ordering of the magnetic rare earth sublattice in the temperature range below 10 K can be detected for  $\text{Eu}_{1-x}\text{Y}_x\text{MnO}_3$ . For comparison the inset of Fig. 7 shows data for pure  $\text{GdMnO}_3$  and  $\text{EuMnO}_3$ . Besides the mentioned differences at low temperatures for  $\text{EuMnO}_3$  an additional contribution at higher temperatures is ob-

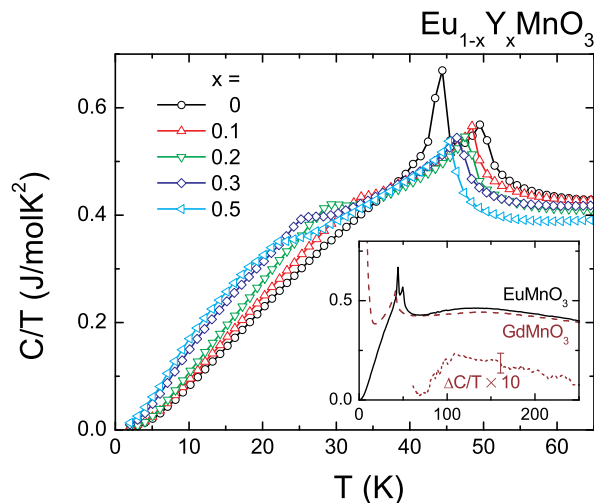


FIG. 7: (Color online) Heat capacity of  $\text{Eu}_{1-x}\text{Y}_x\text{MnO}_3$  plotted as  $C/T$  as a function of temperature. The inset compares the data for pure  $\text{EuMnO}_3$  (solid line) and  $\text{GdMnO}_3$  (dashed line) for temperatures up to 250 K. The dotted line represents the difference multiplied by a factor of 10.

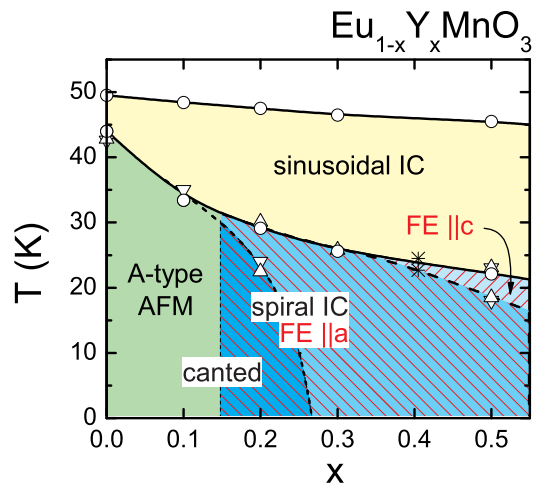


FIG. 8: (Color online)  $(T, x)$ -phase diagram of  $\text{Eu}_{1-x}\text{Y}_x\text{MnO}_3$  for Y-concentrations  $0 \leq x \leq 0.5$ . The data points were obtained from the measurements of the specific heat ( $\circ$ ), the magnetization ( $\nabla$ ), the permittivity ( $\triangle$ ), and from Ref. [25] (\*).

served. This contribution can not be explained by the slight differences of the phonon spectrum because Gd and Eu have very similar masses.  $\Delta C(t)$  shows a broad peak at around 120 K and can be explained by the relatively small splitting of the Eu-multiplet, which also gives rise to the Van-Vleck contribution to the magnetic susceptibility, discussed above.

#### IV. PHASE DIAGRAM

Based on the results shown above, from the magnetic and dielectric measurements as well as from the heat capacity, a detailed  $(x, T)$ -phase diagram can be constructed and is shown in Fig. 8. The paramagnetic regime above  $T_N \approx 45 - 50$  K, is followed by the sinusoidal IC structure of the manganese moments, an interpretation guided by results for  $\text{TbMnO}_3$ <sup>17,23</sup> and  $\text{o-HoMnO}_3$ .<sup>31</sup> For small Y-concentrations,  $x \leq 0.2$ , this incommensurate spin-structure locks into the weakly ferromagnetic A-type CAFM phase. For higher concentrations,  $x \geq 0.3$ , the ground state is ferroelectric but no ferromagnetic component can be found. Obviously, the spin-structure does not lock into the CAFM anymore. However, like in  $\text{TbMnO}_3$  it remains unclear so far, if the magnetic structure still is incommensurate<sup>17</sup> or if a commensurate long wavelength magnetic vector is established.<sup>30</sup> In a small regime around  $x \approx 0.2$  weak ferromagnetism (CAFM) and weak ferroelectricity coexist in contrast to the pure multiferroic rare earth manganites. Regarding the volume of the unit cell, the series  $\text{Eu}_{1-x}\text{Y}_x\text{MnO}_3$  covers the values of  $\text{GdMnO}_3$  and  $\text{TbMnO}_3$ . Pure  $\text{EuMnO}_3$  is not ferroelectric.  $\text{GdMnO}_3$  is ferroelectric along  $a$  in a weak external magnetic field along  $b$ , which destroys the A-type AFM structure.<sup>10</sup> For  $\text{Eu}_{1-x}\text{Y}_x\text{MnO}_3$  a concentration slightly

lower than  $x = 0.2$  probably will reproduce this property of  $\text{GdMnO}_3$ . However, according to Fig. 2 the Eu:Y-system corresponding to  $\text{GdMnO}_3$  should have  $x \approx 0.2$ . This composition is already ferroelectric without magnetic field even though a canted AFM structure persists. Pure  $\text{TbMnO}_3$  is ferroelectric along  $c$ .<sup>10</sup> However, concerning the volume of the unit cell it could not be reproduced by pure single crystalline  $\text{Eu}_{1-x}\text{Y}_x\text{MnO}_3$  close to  $x \approx 0.85$  as shown in Fig. 2. In  $\text{TbMnO}_3$  there is an additional anisotropy due to Tb-ions and Tb-Mn exchange which could lead to the observed electric polarization along the  $c$ -axis. This should be taken into account for the comparison between  $\text{TbMnO}_3$  and  $\text{Eu}_{1-x}\text{Y}_x\text{MnO}_3$  systems. However, the tendency towards a spontaneous ferroelectric component along  $c$  is already indicated also for  $\text{Eu}_{1-x}\text{Y}_x\text{MnO}_3$  at lower Y-concentrations like  $x = 0.5$  (Fig. 6).

It is interesting that only the weak FE component along  $a$  coexists with spontaneous weak ferromagnetism, namely within the concentration range around  $x \approx 0.2$ , while for higher concentrations, where at least an intermediate FE component along  $c$  is detected, no weak ferromagnetism shows up. According to the symmetry properties of the magnetoelectric coupling for the rare earth manganites<sup>12,16,17</sup>, the ferroelectric polarization vector is orthogonal to both, the vector of the magnetic spiral and the magnetic modulation vector, which points along the  $b$  axis.<sup>9</sup> For  $\text{TbMnO}_3$ <sup>17</sup> and analog for the higher Y-concentrations of  $\text{Eu}_{1-x}\text{Y}_x\text{MnO}_3$  the ferroelectric component points along the  $c$ -direction, which is compatible with a spiral vector along  $a$  (i.e. the spins rotating in the  $bc$ -plane). For  $\text{GdMnO}_3$  (in small magnetic fields along  $c$ <sup>21</sup>) and similarly for the concentrations around  $x \approx 0.2$  of  $\text{Eu}_{1-x}\text{Y}_x\text{MnO}_3$ , the ferroelectric component points along the  $a$ -direction. This would be compatible with a spiral vector along  $c$  (i.e. the spins rotating in the  $ab$ -plane). The homogeneous canting of this helicoidal spin structure out of the  $ab$ -plane could then generate the observed ferromagnetic moment along  $c$ .

## V. CONCLUSION

In summary, we have characterized poly- and single-crystalline samples of the system  $\text{Eu}_{1-x}\text{Y}_x\text{MnO}_3$  by means of structural, magnetic, thermodynamic, and di-

electric measurements. In comparison with recently published results for the pure rare earth systems we constructed a  $(T, x)$ -phase diagram for compositions  $x \leq 0.5$ . The ground state  $\text{Eu}_{1-x}\text{Y}_x\text{MnO}_3$  changes from a canted A-type AFM without long range polar order for concentrations  $x < 0.15$  towards a presumably incommensurate spiral magnetic structure coexisting with a ferroelectric component for  $x \geq 0.3$ . For these higher Y-concentrations the orientation of the ferroelectric component changes spontaneously from the  $c$ -axis at higher temperatures towards the  $a$ -axis for low temperatures. The regime with  $P \parallel c$  increases with increasing Y-concentration. In this sense  $\text{Eu}_{1-x}\text{Y}_x\text{MnO}_3$  resembles the development of the ferroelectric orientation with decreasing ionic A-site radius as in the system  $\text{Tb}_{1-x}\text{Gd}_x\text{MnO}_3$ .<sup>32</sup> Hence, all essential magnetoelectric properties existing in the pure rare earth compounds  $\text{GdMnO}_3$  and  $\text{TbMnO}_3$  are reproduced. The influence of the magnetic rare earth seems to be restricted to the distortion of the magnetic structure connected with the magnetic A-site ordering at low temperatures. The modulation of the magnetic structure related to the onset of ferroelectricity is realized due to the Mn sublattice only. However, the contraction of the lattice with increasing  $x$  in  $\text{Eu}_{1-x}\text{Y}_x\text{MnO}_3$  is less effective than estimated from the average ionic A-site radii in comparison to the pure rare earth compounds, which points towards the importance of disorder effects. The latter may also influence the properties in the concentration range around  $x \approx 0.2$  where a finite spontaneous magnetic moment and ferroelectricity coexist. The details of the underlying magnetic structure are not yet verified but it is plausible to expect a spontaneously canted spiral. Such a FM and FE ground state has not been found in the pure rare earth compounds so far and deserves further study.

## Acknowledgments

This work was partly supported by the Bundesministerium für Bildung und Forschung (BMBF) via Grant No. VDI/EKM 13N6917-A, by the Deutsche Forschungsgemeinschaft via Sonderforschungsbereich SFB 484 (Augsburg), and by INTAS and Russian Foundation for Basic Researches N 04-02-16592, 06-02-17514, 04-02-81046-Bel2004.

<sup>1</sup> M. Fiebig, J. Phys. D: Appl. Phys. **38**, R123 (2005).

<sup>2</sup> J. Hemberger, P. Lunkenheimer, R. Fichtl, H.-A. Krug von Nidda, V. Tsurkan, and A. Loidl, Nature **434**, 364 (2005).

<sup>3</sup> P. Lunkenheimer, R. Fichtl, J. Hemberger, V. Tsurkan, and A. Loidl, Phys. Rev. B **72**, 060103(R) (2005).

<sup>4</sup> G. Lawes, A. B. Harris, T. Kimura, N. Rogado, R. J. Cava, A. Aharony, O. Entin-Wohlman, T. Yildirim, M. Kenzelmann, C. Broholm, et al., Phys. Rev. Lett. **95**, 087205

(2005).

<sup>5</sup> T. Lottermoser, T. Lonkai, U. Amann, D. Hohlwein, J. Ihringer, and M. Fiebig, Nature **430**, 514 (2004).

<sup>6</sup> M. Fiebig, T. Lottermoser, D. Fröhlich, A. V. Goitsev, and R. V. Pisarev, Nature **419**, 818 (2002).

<sup>7</sup> N. Hur, S. Park, P. A. Sharma, J. S. Ahn, S. Guha, and S. W. Cheong, Nature **429**, 392 (2004).

<sup>8</sup> T. Kimura, T. Goto, H. Shintani, K. Ishizaka, T. Arima, and Y. Tokura, Nature **426**, 55 (2003).

- <sup>9</sup> T. Goto, T. Kimura, G. Lawes, A. P. Ramirez, and Y. Tokura, *Phys. Rev. Lett.* **92**, 257201 (2004).
- <sup>10</sup> T. Kimura, G. Lawes, T. Goto, Y. Tokura, and A. P. Ramirez, *Phys. Rev. B* **71**, 224425 (2005).
- <sup>11</sup> I. A. Sergienko and E. Dagotto (cond-mat/0508075).
- <sup>12</sup> H. Katsura, N. Nagaosa, and A. V. Balatsky, *Phys. Rev. Lett.* **95**, 057205 (2005).
- <sup>13</sup> C. Ederer and N. A. Spaldin (cond-mat/0602400).
- <sup>14</sup> J. Hemberger, S. Lobina, H.-A. Krug von Nidda, N. Tris-tan, V. Y. Ivanov, A. A. Mukhin, A. M. Balbashov, and A. Loidl, *Phys. Rev. B* **70**, 024414 (2004).
- <sup>15</sup> T. Kimura, S. Ishihara, H. Shintani, T. Arima, K. T. Takahashi, K. Ishizaka, and Y. Tokura, *Phys. Rev. B* **68**, 060403(R) (2003).
- <sup>16</sup> M. Mostovoy, *Phys. Rev. Lett.* **96**, 067601 (2006).
- <sup>17</sup> M. Kenzelmann, A. B. Harris, S. Jonas, C. Broholm, J. Schefer, S. B. Kim, C. L. Zhang, S. W. Cheong, O. P. Vajk, and J. W. Lynn, *Phys. Rev. Lett.* **95**, 087206 (2005).
- <sup>18</sup> A. Pimenov, A. A. Mukhin, V. Y. Ivanov, V. D. Travkin, A. M. Balbashov, and A. Loidl, *Nature Physics* **2**, 97 (2006).
- <sup>19</sup> H. Katsura, A. V. Balatsky, and N. Nagaosa (cond-mat/0602547).
- <sup>20</sup> N. A. Hill and A. Filippetti, *J. Magn. Magn. Mater.* **242**, 976 (1998).
- <sup>21</sup> J. Baier, D. Meier, K. Berggold, J. Hemberger, A. Balbashov, J. A. Mydosh, and T. Lorenz, *Phys. Rev. B* **73**, 100402(R) (2006).
- <sup>22</sup> J. Hemberger, A. Krimmel, T. Kurz, H.-A. Krug von Nidda, V. Y. Ivanov, A. A. Mukhin, A. M. Balbashov, and A. Loidl, *Phys. Rev. B* **66**, 094410 (2002).
- <sup>23</sup> S. Quezel, F. Tcheou, J. Rossat-Mignod, G. Quezel, and E. Roudaut, *Physica B* **86-88**, 916 (1977).
- <sup>24</sup> V. Y. Ivanov, A. A. Mukhin, V. D. Travkin, A. S. Prokhorov, A. M. Kadomtseva, Y. F. Popov, G. P. Vorob'ev, K. I. Kamilov, and A. M. Balbashov, *Phys. Status Solidi B* **243**, 107 (2006).
- <sup>25</sup> K. Noda, M. Akaki, T. Kikuchi, D. Akahoshi, and H. Kuwahara (cond-mat/0512139).
- <sup>26</sup> K. Taylor and M. Darby, *Physics of Rare Earth Solids* (Chapman and Hall Ltd., London, 1972).
- <sup>27</sup> A. Herpin, *Theorie de magnetism* (Presses Universitaires de France, Paris, 1968).
- <sup>28</sup> I. Solovyev, N. Hamada, and K. Terakura, *Phys. Rev. Lett.* **76**, 4825 (1996).
- <sup>29</sup> V. Skumryev, F. Ott, J. M. D. Coey, A. Anane, J.-P. Renard, L. Pinsard-Gaudart, and A. Revcolevschi, *Eur. Phys. J. B* **11**, 401 (1999).
- <sup>30</sup> T. Arima, T. Goto, Y. Yamasaki, S. Miyasaka, K. Ishii, M. Tsubota, T. Inami, Y. Murakami, and Y. Tokura, *Phys. Rev. B* **72**, 100102(R) (2005).
- <sup>31</sup> H. W. Brinks, J. Rodriguez-Carvajal, H. Fjellvag, A. Kjekshus, and B. C. Hauback, *Phys. Rev. B* **63**, 094411 (2001).
- <sup>32</sup> T. Goto, Y. Yamasaki, H. Watanabe, T. Kimura, and Y. Tokura, *Phys. Rev. B* **72**, 220403(R) (2005).